NUMERICAL INVESTIGATION OF CONDENSING FLOW OF LOW PRESSURE STEAM TURBINE AT DIFFERENT FLOW RATE CONDITIONS

by

Kezhen HUANG[a], Lin CAI[b,c*], Jianshu GAO[b], Zhuo LIU[b], and Xinggang YU[b]

[a] China Ship Development and Design Center, Wuhan, China
[b] Key Laboratory of Hydraulic Machinery Transients, Wuhan University, Wuhan, China
[c] School of Power and Mechanical Engineering, Wuhan University, Wuhan, China

Original scientific paper
https://doi.org/10.2298/TSCI17S1161H

The numerical investigation on the wet steam flow in the last two stages of a 1000 MW fossil-fired low pressure steam turbine is presented in this paper. The non-equilibrium model via the classical nucleation theory is employed to simulate the condensing flow of the wet steam. The characteristics of the flow filed from design condition to low volume flow condition are calculated and the static performance of last stage moving blade is also obtained. The development of the back-flow phenomenon is clearly captured through the analysis of the velocity triangle.

Key words: *low volume flow, steam turbine, condensation, windage condition, CFD*

Introduction

The spontaneous condensation of the wet steam in the steam turbine and its influence on the reliability of the unit has been an important research content in the field of steam turbine design. For the difference between electric power peak and valley has been largely increased, to maintain a balance of power supply-demand in power grid, some large capacity units have to participate in the process of peak shaving [1]. If the steam turbine is running in the low-volume-flow (LVF) condition, the temperature in the low pressure part increases. The strength problem of the low pressure cylinder or last stage moving blade (LSB) is also revealed. When the LSB is rotating at the LVF condition, the occurrence of back flow from the exhaust chamber makes entrained drops to a large relative velocity impact blade, which will bring some new problems, including the decrease in stage efficiency, the erosion of the LSB trailing edge [2]. The simulation results using the non-equilibrium model showed that, as the flow rate decreased, not only the quantity of droplets , but also the condensation region was changed [3]. In Sigg [4] experimental and numerical work a good evidence for the accuracy of the CFD model, the results showed that the temperature rise, pressure ratio, and output power agreed well with the experimental date at LVF condition by using the equilibrium phase transition model. Sigg [4] also proved that the development of thee back flow vortex could be clearly seen through the CFD method. Both experimental and numerical studies showed that the generation of vortices had a sequence

* Corresponding author, e-mail: cailin03313@whu.edu.cn

of processes as the low pressure turbine changed to LVF condition [5]. The windage flow field had the main flow meandering distribution in the meridional plane. The process indicated that the generation of vortex was related to the return flow from the exhaust chamber.

In this work, in order to investigate the characteristics of the flow at the stages of the steam turbine low pressure under different working conditions, a non-equilibrium condensation model is employed to describe the two stages of a 1000 MW fossil-fired low pressure steam turbine at different flow ratios, φ. Moreover, the velocity vector, including the flow angle and velocity triangles, is discussed.

Mathematical model

The total stage number of the low pressure steam turbine, studied in the present work, is 6. The S5, R5, S6, R6, and dfffuser zone are main calculation zones for the low pressure steam turbine. The E31 and E32 are the inlet and outlet plane of R6. The parts of the penultimate stage, the last stage and the exhaust chamber surface are considered, as shown in fig. 1. The inlet of S5 is set as the pressure boundary condition with the total pressure and temperature. The opening boundary condition with the given pressure and wetness is applied for diffuser outlet. All the walls are set as adiabatic with no slip wall type.

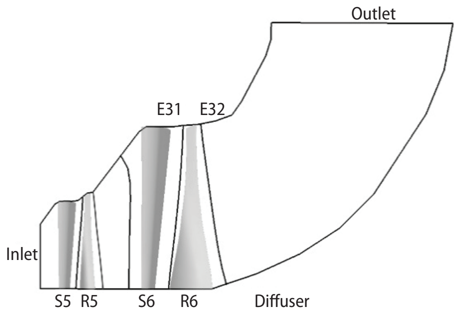

Figure1. Schematic diagram of calculation domain

The CFD software ANSYS CFX 15.0 is adopted for solving the RANS Navier-Stokes equations. The non-equilibrium model with the condensation droplet characteristics can be obtained in [3]. The number of the fine droplets formed is given:

$$J = \left[\frac{q_c}{1+\eta} \left(\frac{2\sigma}{\pi m^3} \right)^{\frac{1}{2}} \right] \left[\frac{\rho_v}{\rho_l} \exp\left(-\frac{4\pi r^{*2}\sigma}{3KT_c} \right) \right] \tag{1}$$

where $q_c = 1$, and σ, m, ρ_v, ρ_l, K, and T_c are the surface tension of droplets, mass of the water molecule, densities of the vapor and water liquid, Boltzmann's constant and temperature of vapor, respectively.

The Kantrowitz's non-isothermal correction factor η is given:

$$\eta = 2\frac{\gamma - 1}{\gamma + 1} \frac{L}{\mathrm{R}T_c} \left(\frac{L}{\mathrm{R}T_c} - \frac{1}{2} \right) \tag{2}$$

where γ is the specific heat capacity of vapor, L – the latent heat, and R – the gas specific constant.

The critical droplet radius r^* is defined by:

$$r^* = \frac{2\sigma}{\rho_l \Delta G_c} \tag{3}$$

where ΔG_c is the bulk Gibbs free energy change of gas phase depending on the equation of state.

The droplet-growth rate derived from the heat transfer surrounding droplets is given:

$$\frac{\mathrm{d}r}{\mathrm{d}t}=\frac{k_c}{r\rho_d(1+c\,\mathrm{Kn})}\left(\frac{T_d-T_c}{h_c-h_d}\right) \tag{4}$$

where T_d and T_c are, respectively, the droplet and the vapor temperature, Kn – the Knudsen number, k_c – the thermal conductivity of the vapor, h_c and h_d are the droplet and the vapor static enthalpy, respectively, and c is an empirical factor.

When using the non-equilibrium model, only one condensed phase model in multiple stages flow field calculation would be inaccurate. It is suggested that using *source specific* method will improve accuracy. In this work, the gas phase (steam vapor) is defined as P1, and there is only one of it, P2 is a condensed phase that can only have its source location in stator 5, and P3 only in rotor 5, P4 only in stator 6, P5 in rotor 6 and diffuser zone. The SST k-ω model is suitable for the LVF condition in the steam turbine, see, [3, 6]. The hexahedron cells are used for the discrete calculation region as is shown in fig. 2.

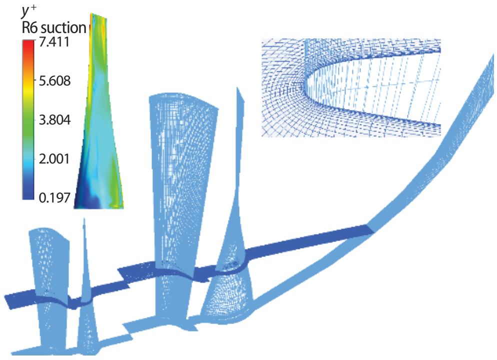

Figure 2. The grid structure and y^+ distribution of R6
(*for color image see journal web site*)

The computational grid has about the 2.6 million elements in total. The near-wall grid is densified in order to ensure that $y^+<10$. The experimental data of the wet steam flow in cascade and nozzle were carried out in [7-9]. The 2-D stator cascade measurements are particularly relevant to low pressure steam turbine conditions [7]. They are utilized to validate the non-equilibrium condensation model in this work. The Moore's nozzle is also designed at the last stage of the low-pressure-steam turbine. For more details, see [6].

Results and discussion

Pressure ratio, temperature rise, and output power

Two monitor points are set in front and behind the LSB tip, as shown in fig. 3.

With the decrease of the inlet pressure, the flow rate of the steam flowing into the steam turbine decreases slowly. With the decrease of the flow ratio, φ, to 0.26 (the critical value of the flow ratio in the work), the pressure ratio is close to 1.0. With the decrease of the flow ratio the LSB of the steam turbine begins to compress the steam (so-called *windage condition*).

Figure 4 shows the relationship between the flow ratio and the output power coefficient of R6.

The output power decreases with the decrease of the flow ratio. When the flow ratio is close to 0.22, the final output power is 0. The

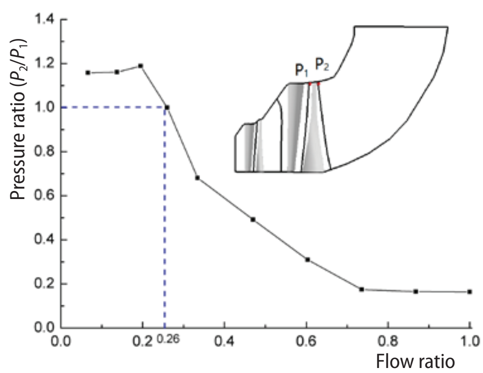

Figure 3. Pressure ratio over the tip of R6 at the flow ratios φ

whole blade of the R6 still has the power capability when the LSB tip zone begins to compress the fluid. The tip zone of LSB is in the state of the power consumption. However, with the further decrease of the flow ratio the back flow region in R6 is gradually expanded, and the total output power is lower than 0.

In the windage condition, the flow temperature of the LSB increases significantly. The comparison of temperature distributions of flow ratios $\varphi = 1.0$ and $\varphi = 0.66$ in the plane E31 is given in fig. 5.

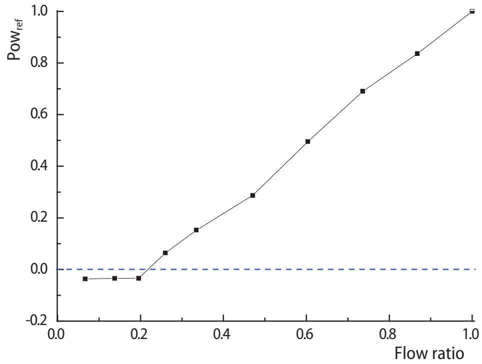

Figure 4. Power output of R6 at the different flow ratios

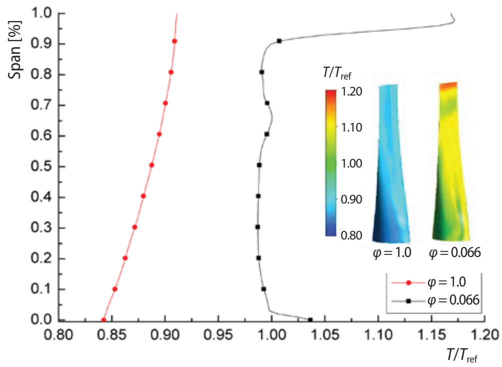

Figure 5. Temperature distributions of the flow ratios $\varphi = 1.0$ and $\varphi = 0.66$ in the plan E31
(*for color image see journal web site*)

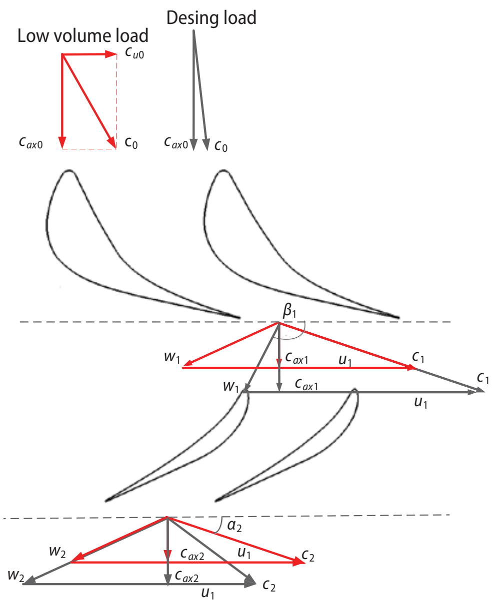

Figure 6. Velocity triangles during design and low volume rate operation of a stage:
c – the velocity, c_{ax} – axial velocity component, c_{u0} – tangential velocity component, w – the relative velocity, u – circumferential velocity, 0, 1, 2 are, respectively. the stator inlet, rotor inlet and rotor outlet (*for color image see journal web site*)

The value T/T_{ref} (dimensionless temperature) gradually increases along the radial direction. As the flow ratio decreases to 0.66, the output power of R6 is below 0. The high temperature of the LSB, caused by the LVF condition, would bring the strength problem to low pressure cylinder or LSB. When the temperature monitor value is higher than 65 °C, the spry nozzle should be opened in time.

The velocity filed

Figure 6 displays the variations of velocity triangles from the design to LVF conditions.

As the flow ratio decreases, the axial velocity component decreases (c_{1ax} from black line to red line). Meanwhile, the rotating speed, u, is unchanged, which makes the moving blade inlet velocity, w_1, decrease, and also results in an increase of the flow angle, β_1.

Figure 7 illustrates the c_{1ax} distribution at the different flow ratios.

Figure 8 illustrates the flow angle, β_1, distribution at different flow ratios.

Figure 9 shows the c_{2ax} distribution of E32 at the different flow ratios.

Figure 10 shows meridional streamline of five typical conditions.

Figure 11 indicates the surface streamline distribution of LSB suction side at different flow ratios.

The flow separation in two aspects is illustrated in fig.12.

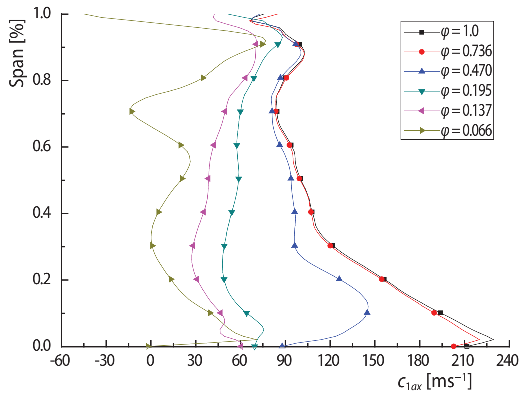

Figure 7. The c_{1ax} distribution of E31 at different flow ratios
(*for color image see journal web site*)

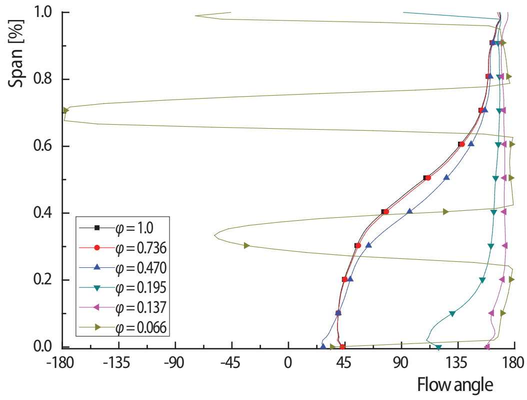

Figure 8. Flow angle of the R6 distribution at different flow ratios
(*for color image see journal web site*)

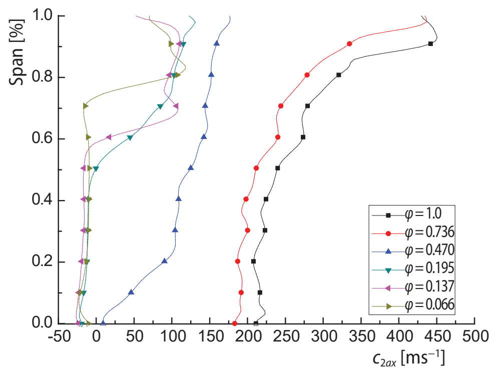

Figure 9. The c_{2ax} distribution of E32 at different flow ratios
(*for color image see journal web site*)

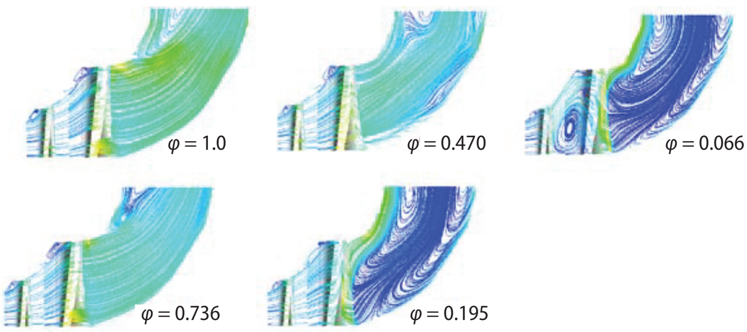

Figure 10. Meridional streamlines at the different flow ratios
(*for color image see journal web site*)

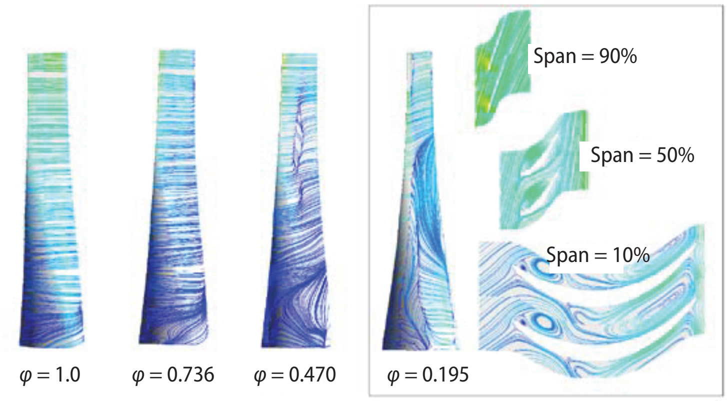

Figure 11. The surface streamline of R6 suction side at different flow ratios
(*for color image see journal web site*)

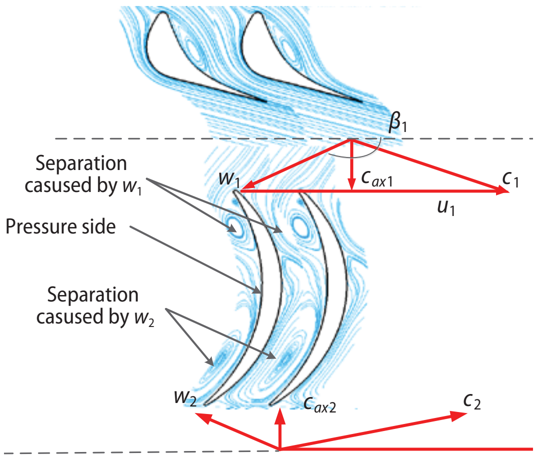

Figure 12. The velocity triangle of LSB at φ = 0.195; Span = 0.1
(*for color image see journal web site*)

Conclusions

In this paper, the CFD numerical method is used to study wet steam flow in the last two stages of a 1,000 MW fossil-fired low pressure steam turbine. By solving the RANS N-S equations with non-equilibrium condensation model, several conditions of the flow field at different flow ratios have been calculated. The generation and development process of windage condition have been obtained and discussed. The velocity flied, including flow inlet angle and velocity triangles have also been analyzed. The condensation droplet characteristics have been discussed.

As flow ratios decreases, the pressure ratio of LSB tip and output power decrease. When the pressure ratio is equal to 1, the LSB still has power capability, but reversed flow from exhaust chamber to LSB has already occurred near the blade root zone. With the further decrease of flow ratios, the output power of LSB is negative, the LSB is completely in windage condition. The flow inlet angle of LSB decreases with the decrease of flow ratios, the root zone at first presents the separation flow. Compared to the c_{1ax}, the c_{2ax} near the root zone at first appears negative in early windage condition (such as when $\varphi = 0.195$ in this paper), while the inlet velocity c_{1ax} is still greater than 0. This makes two obvious separation bubbles generated from the root zone. Under the action of centrifugal force, the flow of the steam in LSB flow channel has an obvious radial movement. With the further decrease of φ, c_{1ax} at the root of LSB gradually reduces to a negative value, leading to the reversed flow moving towards S5 direction.

Acknowledgment

The authors would like to express their gratitude to the financial support of the Fundamental Research Funds for the Central Universities (Grant No. 413000011, 413000062).

Nomenclature

c, w – velocity, [ms^{-1}]
Span – dimensionless blade heigh, [–]
Pow$_{ref}$ – Power/Power$_{design\ point}$, [–]
T/T_{ref} – dimensionless temperature, [–]
u – circumferential velocity, [ms^{-1}]

Greek symbols

α, β – flow angle
φ – mass flow rate/mass flow rate design point

Acronyms

LSB – last stage moving blade, [–]
LVF – low volume flow, [–]

References

[1] Gu, Y. J., *et al.*, Overall Review of Peak Shaving for Coal-Fired Power Units in China, *Renewable and Sustainable Energy Reviews*, *54* (2016), Feb., pp. 723-731
[2] Wang, W. Z., *et al.*, Failure Analysis of the Final Stage Blade in Steam, *Engineering Failure Analysis*, *14* (2007), 4, pp. 632-641
[3] Gerber, A. G., *et al.*, Predictions of Non-Equilibrium Phase Transition in a Model Low-Pressure Steam Turbine, *Proc, IMechE Part A: J. Power and Energy*, *221* (2007), 6, pp. 825-835
[4] Sigg, R., *et al.*, Numerical and Experimental Investigation of a Low-Pressure Steam Turbine During Windage, *Proc. IMechE Part A: J. Power and Energy*, *223* (2009), 6, pp. 697-708
[5] Senoo, S., *et al.*, Computations for Unsteady Compressible Flows in a Multistage Steam Turbine with Steam Properties at Low Load Operations, *Journal of Engineering for Gas Turbines and Power*, *133* (2011), 10, pp. 103-113
[6] Yu, X., *et al.*, Numerical Investigation of Condensing Flow in the Last Stage of Low-Pressure Nuclear Steam Turbine, *Nuclear Engineering and Design*, *275* (2014), 8, pp. 197-204
[7] Kermani, M. J., *et al.*, A General Formula for the Evaluation of Thermodynamic and Aerodynamic Losses in Nucleating Steam Flow, *International Journal of Heat and Mass Transfer*, *46* (2003), 17, pp. 3265-3278
[8] White, A. J., *et al.*, Experimental Validation of Condensing Flow Theory for a Stationary Cascade of Steam Turbine Blades, *Philos. Trans. R. Soc.*, *354* (1996), 1704, pp. 59-88
[9] Moore, M. J., *et al.*, *Predicting the Fog-Drop Size in Wet-Steam Turbines*, Institute of Mechanical Engineering, London, 1974, Vol. 73, pp. 101-109

Paper submitted: March 10, 2017
Paper revised: May 1, 2017
Paper accepted: May 12, 2017